

## Photon Drag Effect due to Berry Curvature

Hiroyuki Kurosawa,<sup>1,2,\*</sup> Kei Sawada,<sup>3</sup> and Seigo Ohno<sup>1</sup>

<sup>1</sup>*Department of Physics, Graduate School of Science, Tohoku University, 6-3 Aramaki Aoba, Sendai 980-8578, Japan*

<sup>2</sup>*National Institute for Materials Science (NIMS), 1-1 Namiki, Tsukuba, Ibaraki 305-0044, Japan*

<sup>3</sup>*RIKEN SPring-8 Center, 1-1-1, Kouto, Sayo-cho, Sayo-gun, Hyogo 679-5148, Japan*

(Received 16 February 2016; revised manuscript received 19 May 2016; published 15 August 2016)

A theoretical investigation reveals that the photon drag effect (PDE) is induced in a grating slab with deformation by the Berry curvature in phase space. It drifts the momentum of light, and gives asymmetric PDE signals in momentum space. Large PDE signals are observed even near the  $\Gamma$  point. This characteristic agrees well with our theoretical results.

DOI: 10.1103/PhysRevLett.117.083901

The interaction between light and matter has been a fascinating topic in physics. Optical fields have an oscillating nature that gives ac responses of electrons in most linear and nonlinear processes. It is interesting to see if electrons have a dc response to optical fields. Such a response is realized by using  $\omega - \omega$  nonlinear effects [1]. A nonlinear dc current is induced in noncentrosymmetric materials by the  $\chi^{(2)}$  process, known as the photogalvanic effect [2,3]. Another mechanism inducing a nonlinear dc current is the quadrupole nonlinearity in centrosymmetric materials, known as the photon drag effect (PDE).

The PDE is originally known as the voltage due to momentum transfer from light to a charged carrier and has been investigated in semiconductors, carbon nanotubes, and graphene [4–9]. In those materials, the photovoltage is induced by an asymmetric momentum distribution in an electric band structure. Another mechanism of the PDE is realized in a simple metal [10] through the quadrupole responses by the Lorentz force on an electric dipole [11–13]. Controlling such a force can lead to a new PDE mechanism. Here, we focus on a fictitious Lorentz force due to Berry curvatures.

Berry curvatures play the role of effective magnetic fields for light and are an origin of the Berry phase. The Berry phase first appeared as a geometric property of the wave function in quantum systems, but its concept is also applicable even for classical wave physics. On the basis of this idea, the Berry phase is extensively studied in relation to the topological state in metamaterials [14]. Onoda and Ochiai theoretically showed that the Berry curvature in momentum space gives rise to a vortexlike Lorentz force, named an optical tornado [15]. Those studies are focused on the geometrical aspect of the wave function in momentum space. Here, we focus on another Berry curvature, defined in real and momentum spaces, namely phase space. The Berry curvature in phase space has also been investigated theoretically and experimentally as gigantic x-ray translations in deformed crystals [16–18]. In the optical region, there is no study related to the Berry curvature associated with spatial deformation.

In this Letter, we theoretically and experimentally show that the Berry curvature in phase space appears in the nonlinear response and gives rise to a novel PDE.

Let us consider the second-order nonlinear current induced in a metallic film, shown in Fig. 1(a), where a wave packet with  $s$  polarization is incident to a deformed grating on the film. From the equation of motion, we can derive the nonlinear dc current to be  $\mathbf{J}_{\omega-\omega} = q/(m\gamma)\mathbf{F}_{\omega-\omega}$ , where  $q$  is the charge,  $m$  is the mass, and  $\gamma$  is the damping factor of an electron [19].  $\mathbf{F}_{\omega-\omega} = (1/2)\text{Re}[\alpha(\omega)\{(\tilde{\mathbf{E}} \cdot \nabla)\tilde{\mathbf{E}}^* + \tilde{\mathbf{E}} \times (\nabla \times \tilde{\mathbf{E}}^*)\}]$  is the nonlinear dc force, where  $\alpha(\omega) = \alpha_r(\omega) + i\alpha_i(\omega)$  is the polarizability of a metal and  $\tilde{\mathbf{E}}$  is the complex amplitude of the electric field. This force consists of the gradient and the scattering forces. The gradient force, defined as  $\mathbf{F}^{\text{Grad}} = [\alpha_r(\omega)/4]\nabla|\tilde{E}_s(\mathbf{r})|^2$ , vanishes due to the periodic boundary condition when integrated along the periodic direction [20]. The scattering force is defined as

$$\begin{aligned} \mathbf{F}^{\text{Scat}} &= \frac{\alpha_i(\omega)}{2} \text{Im}\{\tilde{E}_s^*(\mathbf{r})\nabla\tilde{E}_s(\mathbf{r})\} \\ &= \frac{\alpha_i(\omega)}{2} I[\mathbf{k}|\tilde{U}(\mathbf{r})|^2 + \text{Im}\{\tilde{U}^*(\mathbf{r})\nabla\tilde{U}(\mathbf{r})\}], \quad (1) \end{aligned}$$

where  $\tilde{E}_s(\mathbf{r}) = \sqrt{I}e^{i\mathbf{k}\cdot\mathbf{r}}\tilde{U}(\mathbf{r})$  is the  $s$ -polarized component of the electric field,  $I$  is the light intensity, and  $\tilde{U}(\mathbf{r})$  is a normalized periodic function satisfying  $\tilde{U}(\mathbf{r} + \mathbf{a}) = \tilde{U}(\mathbf{r})$ . Here,  $\mathbf{a}$  is the lattice vector of the grating. The scattering force is related to  $\alpha_i(\omega)$  and the wave vector  $\mathbf{k}$  and represents the momentum transfer due to photon absorption, which is our focus. We assume that the wave function  $\tilde{U}(\mathbf{r})$  is transformed into  $\tilde{U}(\mathbf{r} - \mathbf{u}(\mathbf{r}))$  in the presence of the deformation [16]. Thus, the second term in the angle bracket of Eq. (1) is transformed into  $\text{Im}\{\tilde{U}^*(\mathbf{r} - \mathbf{u}(\mathbf{r}))\nabla\tilde{U}(\mathbf{r} - \mathbf{u}(\mathbf{r}))\} \approx \text{Im}\{\tilde{U}^*(\mathbf{r})\nabla\tilde{U}(\mathbf{r})\} \cdot (\hat{1} - \partial\mathbf{u}(\mathbf{r}_c)/\partial\mathbf{r}_c)$ , where  $\hat{1}$  is the second rank identity tensor and we used the approximation  $\mathbf{u}(\mathbf{r}) \approx \mathbf{u}(\mathbf{r}_c)$ . Here,  $\mathbf{r}_c$  is the center position of the wave packet. The scattering force gives the PDE voltage to be

$$V_a = \frac{1}{nqS_a} \int dr F_a^{\text{Scat}}(\mathbf{r})$$

$$= V_a^0 + \frac{I}{2nqS_a} \alpha_i(\omega) \left( \int d\mathbf{k}_c \cdot \Omega_{rk} \right)_a, \quad (2)$$

where  $V_a^0$  is the PDE voltage due to a perfect crystal,  $n$  is a charge density,  $S_a$  is the cross section of the metallic film perpendicular to the  $a$  direction, and  $\mathbf{k}_c$  is the wave vector of the wave packet center. The Berry curvature is defined as  $(\Omega_{rk})_{ab} := \langle \partial_{r_a} \tilde{U}(\mathbf{r}) | i \partial_{k_b} \tilde{U}(\mathbf{r}) \rangle - \langle \partial_{k_b} \tilde{U}(\mathbf{r}) | i \partial_{r_a} \tilde{U}(\mathbf{r}) \rangle$ . In the following, we consider the second term of Eq. (2) in detail.

Let us introduce the theory of wave-packet propagation in a crystal with a spatial deformation  $\mathbf{u}(\mathbf{r})$ . The equations of motion for the wave packet are as follows [16]:

$$\frac{d\mathbf{r}_c}{dt} = \frac{\partial \omega}{\partial \mathbf{k}_c} - \Omega_{kr} \cdot \frac{d\mathbf{r}_c}{dt}, \quad (3)$$

$$\frac{d\mathbf{k}_c}{dt} = -\frac{\partial \omega}{\partial \mathbf{r}_c} + \Omega_{rk} \cdot \frac{d\mathbf{k}_c}{dt}. \quad (4)$$

In Eq. (3),  $\Omega_{kr}$  is the transpose of  $\Omega_{rk}$ . Near the  $\Gamma$  point, this Berry curvature tensor is represented by  $\Omega_{k_a r_b} = f_{k_a}(\mathbf{k}) g_{r_b}(\mathbf{r})$ , where

$$f_{k_a}(\mathbf{k}) = \pm \frac{(\Delta\omega)^2 (c/\sqrt{\epsilon^0}) (\mathbf{e}_{\mathbf{k}+\mathbf{G}} - \mathbf{e}_{\mathbf{k}-\mathbf{G}})_a}{2[(\Delta\omega)^2 + (\omega_{\mathbf{k}+\mathbf{G}} - \omega_{\mathbf{k}-\mathbf{G}})^2]^{3/2}}, \quad (5)$$

$$g_{r_b}(\mathbf{r}) = \frac{\partial \{2\mathbf{G} \cdot \mathbf{u}(\mathbf{r})\}}{\partial r_b}. \quad (6)$$

Here,  $\Delta\omega$  is the photonic band gap and  $\epsilon^0$  is the zeroth-order Fourier component of the periodic structure.  $\mathbf{e}_{\mathbf{k}} = \mathbf{k}/|\mathbf{k}|$  is a unit vector and  $\omega_{\mathbf{k}} = c|\mathbf{k}|/\sqrt{\epsilon^0}$ .  $\mathbf{G}$  is the reciprocal lattice vector of the crystal. The double sign  $\pm$  in Eq. (5) corresponds to the lower and upper bands, respectively [16]. Thus, the Berry curvature  $\Omega_{k_a r_b}$  is maximum at the  $\Gamma$  point  $\mathbf{k} = 0$ , and is prominent in the case of the narrow photonic band gap.

Following the formulation of the Berry curvature around the  $\Gamma$  point, we will consider the relation between the Berry curvature and the PDE voltage  $V_a$ . When the wave packet with wave vector  $\mathbf{k}_c^0$  is shined to the metal-dielectric (MD) grating slab as shown in Fig. 1(b), the wave packet couples with the eigenmode of the deformed grating, and refracts slightly. From Eq. (4), this refraction is due to the momentum variation, represented by the Berry curvature to be  $\delta\mathbf{k}_c = \int d\mathbf{k}_c \cdot \Omega_{rk}$ . From Eq. (3), the Berry curvature also shifts the center position of the wave packet. The wave packet is partially absorbed by the free carriers and transfers the momentum to the carriers. As a result, a nonlinear current is induced along the trajectory of the center position, resulting in the PDE voltage described by  $V_a$ .

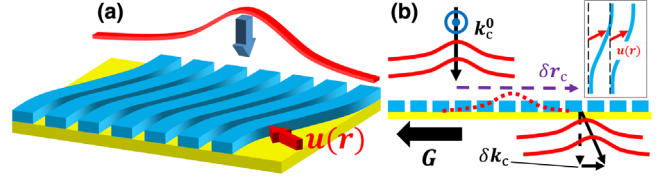


FIG. 1. (a) Deformed dielectric grating on a metallic film. The deformation  $\mathbf{u}(\mathbf{r})$ , defined in Ref. [16], is drawn by a red arrow. The red and blue curves indicate the wave packet and the dielectric grating with deformation, respectively. (b) Translation and refraction due to the Berry curvature. The position shift and refraction are indicated by  $\delta\mathbf{r}_c$  and  $\delta\mathbf{k}_c$ , respectively. The inset shows the top view of the deformed grating.

Equation (2) explicitly shows that the momentum variation due to the Berry curvature,  $\delta\mathbf{k}_c$ , is the source for the PDE.

The PDE voltage  $V_a$  is from two contributions. One is a perfect crystal, and the other is the Berry curvature. Therefore, we need to separate the PDE due to the Berry curvature from that of the perfect crystal. The MD grating slab needs to have an inversion center even in the presence of the deformation. In the absence of the inversion center, the broken space inversion symmetry (SIS) of the perfect crystal would induce the PDE voltage [21,22], but it is out of scope of this Letter. In addition to the SIS of the deformed grating, the parity of the electromagnetic (EM) fields also plays an important role in the PDE. We reveal the relation between the parity and the deformation. An eigenmode at the  $\Gamma$  point is classified into an antisymmetric mode with an even parity and a symmetric mode with an odd one. We consider the parity of the electric field in the presence of the deformation:  $\mathcal{P}_{\parallel} \tilde{E}_s(\mathbf{r} - \mathbf{u}(\mathbf{r})) = \tilde{E}_s(-\mathbf{r} - \mathbf{u}(-\mathbf{r})) = \pm \tilde{E}_s(\mathbf{r} - \mathbf{u}(\mathbf{r}))$ , where  $\mathcal{P}_{\parallel}$  is the parity transform operator in the grating plane. The double sign  $\pm$  indicates the even and odd parity, respectively. Expanding  $\tilde{E}_s(\mathbf{r} - \mathbf{u}(\mathbf{r}))$  to the first order,  $\tilde{E}_s(\mathbf{r} - \mathbf{u}(\mathbf{r})) \approx \tilde{E}_s(\mathbf{r}) - \mathbf{u}(\mathbf{r}) \cdot \nabla \tilde{E}_s(\mathbf{r})$ , and considering the parity transform in the absence of the deformation,  $\mathcal{P}_{\parallel} \tilde{E}_s(\mathbf{r}) = \tilde{E}_s(-\mathbf{r}) = \pm \tilde{E}_s(\mathbf{r})$ , we obtain the following relation:

$$[\mathbf{u}(\mathbf{r}) - \mathbf{u}(-\mathbf{r})] \cdot \nabla \tilde{E}_s(\mathbf{r}) = 0. \quad (7)$$

Equation (7) is reduced to  $\mathbf{u}(\mathbf{r}) \cdot \nabla \tilde{E}_s(\mathbf{r}) = 0$ , when the EM fields are spatially symmetric. Thus, the effect of the deformation does not appear within the first order approximation under the spatially symmetric mode. Therefore, we conclude that the PDE due to the Berry curvature is observable under the excitation of the spatially antisymmetric mode at the  $\Gamma$  point. In what follows, we experimentally demonstrate the PDE due to the Berry curvature in a deformed MD grating slab.

We prepared MD grating slabs with and without deformation as shown in Figs. 2(a)–2(c). The dielectric gratings that comprise the electron beam resist (ZEP520A, Zeon Corporation) are on a Au film. Deformation was introduced

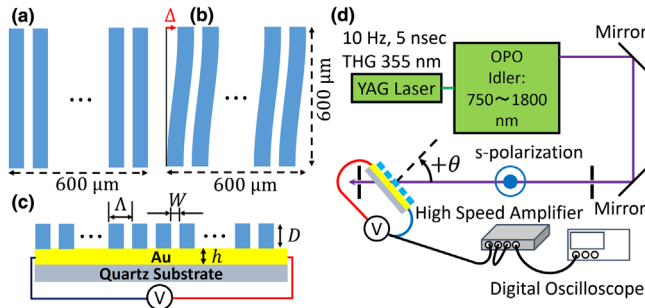


FIG. 2. Schematic of the nondeformed (a) and the deformed (b) MD grating slabs on a Au thin film. The patterned area is  $600 \mu\text{m}$  squared. (c) Cross section of the MD grating slabs. The period  $\Lambda$ , width of the grooves  $W$ , and height  $D$  of the MD grating slabs are 800, 200, and 300 nm, respectively. The thickness of the Au film  $h$  is 40 nm. (d) Schematic of the experimental setup for the PDE voltage measurement.

by electron beam lithography. We drew the deformed line so that the end point, the left bottom edge of the grating, and the middle point are in the same spline cubic interpolated line. The deviation at the end point of the deformed line from the nondeformed one is  $\Delta = 1.2 \mu\text{m}$ . Figure 2(d) shows the schematic of the experimental setup for the PDE voltage measurement. We used an optical parametric oscillator (OPO) pumped by a frequency-tripled Nd doped YAG (yttrium aluminum garnet) laser as a light source. The repetition rate and the pulse width were 10 Hz and 5 ns, respectively. We introduced an *s*-polarized (electric field parallel to the grooves) laser with an incident angle  $\theta$  and an intensity of approximately  $0.55 \text{ MW}/\text{cm}^2$  to the MD grating slabs. Under these conditions, we measured the voltage across the structure, which was amplified by a high speed amplifier with a gain of 125 and observed through a digital oscilloscope.

The angle resolved reflectivity was measured to characterize the linear optical response of the MD grating slabs. Figures 3(a) and 3(b) show the spectra measured from the deformed structure, and calculated for the nondeformed structure, respectively. We found some dispersive features depending on both the energy and incident angle. This feature is a consequence of the resonance associated with the grating. To assign the resonance, we performed a numerical calculation based on the scattering matrix method [23,24]. Figure 3(c) shows the calculated magnetic field at the  $\Gamma$  point on the upper band. The field distribution is strongly enhanced in the dielectric region. From this feature, we assigned this resonance as a waveguide mode. We also confirmed that the measured reflectivity spectra of the nondeformed structure have the same feature as that of the deformed structure (not shown). In the photonic band structure, the upper and lower bands are active and forbidden at the  $\Gamma$  point, respectively. This is a characteristic of the structure with the SIS. Moreover, we find that the upper and lower bands correspond to asymmetric and

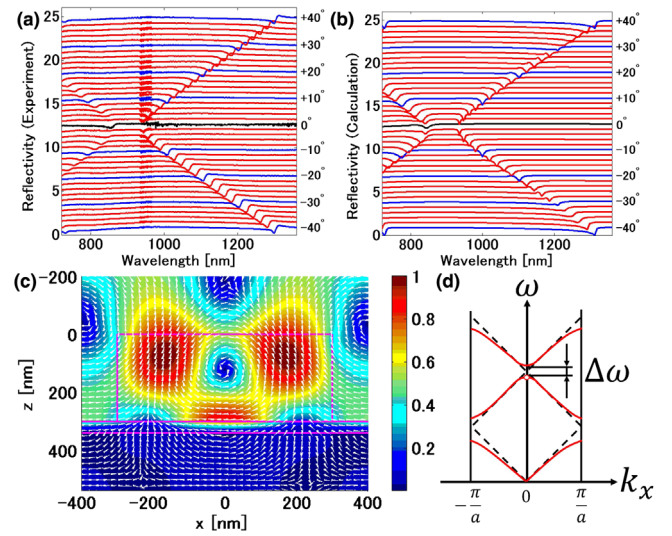


FIG. 3. (a) Measured angle resolved reflectivity spectra from the deformed MD grating. (b) Calculation result of the angle resolved reflectivity spectra of the nondeformed MD grating. (c) Snapshot of the magnetic field at the  $\Gamma$  point of the third band. The colors and the arrows indicate the intensity and the direction of the magnetic field, respectively. (d) Schematic of the band structure. The second band is forbidden at the  $\Gamma$  point.

symmetric modes, respectively. Therefore, the SIS of the deformed structure is not broken; thus, the occurrence of the PDE is not normally expected in the deformed structure at the  $\Gamma$  point. Figure 3(d) shows the schematic of the photonic band structure. The photonic band gap necessary for the shift of the wave packet is estimated to be 0.1 eV, which is clearly found in the experimental and numerical results.

Figure 4(a) shows the PDE voltage spectra at the incident angles from  $-1^\circ$  to  $+1^\circ$  in the nondeformed MD grating slab. Figures 4(b)–4(d) show those of the incident angles from  $\pm 0.1^\circ$ ,  $\pm 1^\circ$ , and  $\pm 10^\circ$  in the deformed grating, respectively. On the spectra around the wavelength of 860 nm in Figs. 4(b) and 4(c), the PDE voltage remains significantly large. This feature corresponds to the excitation of the waveguide mode on the upper band at the  $\Gamma$  point, and is consistent with our theory. Moreover, the PDE voltage at the incident angle  $+1^\circ$  exhibited a positive sign around the wavelength of 860 nm, which indicates that the electrons in the metallic film are attracted opposite to the incident direction due to the Berry curvature. Conversely, we observed a symmetric signal with respect to the incident angle around the wavelength of 940 nm in Fig. 4(c) corresponding to the waveguide mode excitation of the lower band. Because the EM fields for the symmetric waveguide mode are robust to the deformation, the Berry curvature does not affect the PDE in the lower band. The angle dependence of the PDE voltage also can be elucidated from our theory. The Berry curvature  $\Omega_{kr}$  can be regarded as a fictitious magnetic field induced by a monopole in phase space and becomes maximum at the

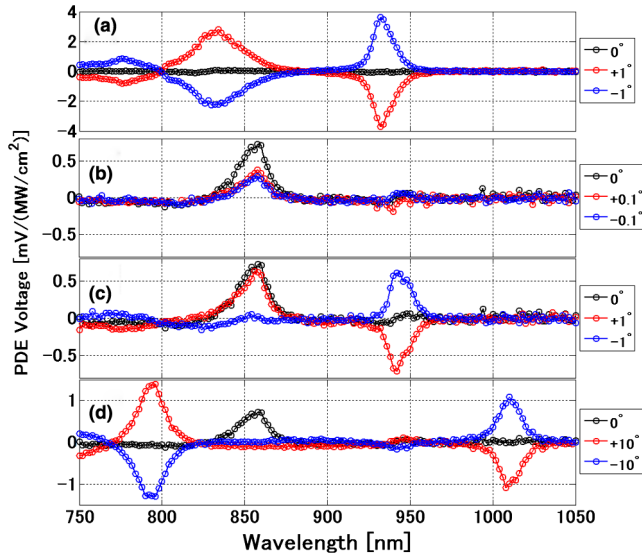


FIG. 4. (a) Observed PDE voltage spectra of the nondeformed structure at the incident angles of  $\pm 1^\circ$ . Observed PDE voltage spectra of the deformed structure at the incident angles of (b)  $\pm 0.1^\circ$ , (c)  $\pm 1^\circ$ , and (d)  $\pm 10^\circ$ .

$\Gamma$  point of the photonic band  $|\mathbf{k} + \mathbf{G}| = |\mathbf{k} - \mathbf{G}|$ . In other words, the effect of the Berry curvature on the PDE becomes prominent only near the Brillouin edge, which is consistent with our experimental results of the angle dependence.

In addition to the Berry curvature, we further consider the relation between the observed PDE voltage and the SIS. As is clear from the symmetry of the nondeformed grating, the observed voltage spectra exhibited symmetric responses with respect to the incident angles. On the other hand, when the structure is deformed and the incident angle is almost normal, the observed voltage spectra are no longer symmetric with respect to the incident angle [Figs. 4(b) and 4(c)]. Moreover, the asymmetric behavior was observed only in the upper photonic band as is shown in Fig. 4(c). However, this feature vanished when the incident angle is  $\pm 10^\circ$ . This means that the PDE voltage associated with the deformation appears only in the upper photonic band near the  $\Gamma$  point. At incident angles of  $\pm 10^\circ$  [Fig. 4(d)], the observed spectra were symmetric in both the nondeformed (not shown) and deformed structures. From the wavelengths of 820 to 950 nm, we find a small but significant voltage in the deformed structures, which is attributed to the PDE induced by diffraction [22]. The PDE voltage in the wavelength range is symmetric. This feature also indicates that the SIS of the deformed MD grating slab is not broken. Thus, we conclude that the influence of the deformation on the PDE voltage was observed only near the  $\Gamma$  point of the upper band, which is attributed to the Berry curvature associated the spatial deformation.

In summary, we have theoretically and experimentally investigated the second-order nonlinear optical response in a deformed crystal. In the deformed crystal, the momentum

variation of the light is caused by the Berry curvature, resulting in the PDE voltage. Following our theory, we prepared deformed and nondeformed MD grating slabs with a waveguide mode resonance. We observed a significant PDE signal near the  $\Gamma$  point only in the deformed structure. The observed signal is well elucidated from our theory, representing the signature of the optical nonlinearity induced in the deformed crystal. Our findings can be extended to other nonlinear phenomena such as second harmonic and terahertz wave generations. Moreover, the PDE voltages in the present study are dynamically controllable by modulating the deformation, leading to dynamical optical devices. Thus, the present study paves the way for controlling the optical nonlinearity in an artificial structure by the Berry curvature in phase space.

The authors are grateful to Professor Masayuki Yoshizawa for fruitful discussion. We also acknowledge Kazuyuki Nakayama, Teruya Ishihara, and Makoto Saito. H. K. is supported by the Japan Society for the Promotion of Science (JSPS). This work is partly supported by Grants-in-Aid for Scientific Research No. 22109005, No. 26289120, and No. 26287065 from the Ministry of Education, Culture, Sports, Science and Technology (MEXT), Japan.

\*Present address: Advanced ICT Research Institute, National Institute of Information and Communications Technology (NICT), Kobe, Hyogo 651-2492, Japan.  
hiroyuki96kurosawa@gmail.com

- [1] Y. R. Shen, *The Principles of Nonlinear Optics* (Wiley, New York, 1984).
- [2] O. E. Alon, *Phys. Rev. B* **67**, 121103 (2003).
- [3] G. Wachter, S. A. Sato, I. Floss, C. Lemell, X.-M. Tong, K. Yabana, and J. Burgdorfer, *New J. Phys.* **17**, 123026 (2015).
- [4] A. F. Gibson, M. F. Kimmitt, and A. C. Walker, *Appl. Phys. Lett.* **17**, 75 (1970).
- [5] R. Loudon, S. M. Barnett, and C. Baxter, *Phys. Rev. A* **71**, 063802 (2005).
- [6] P. A. Obraztsov, T. Kaplas, S. V. Garnov, M. Kuwata-Gonokami, A. N. Obraztsov, and Y. P. Svirko, *Sci. Rep.* **4**, 4007 (2014).
- [7] G. M. Mikheev, A. G. Nasibulin, R. G. Zonov, A. Kaskela, and E. I. Kauppinen, *Nano Lett.* **12**, 77 (2012).
- [8] M. V. Entin, L. I. Magarill, and D. L. Shepelyansky, *Phys. Rev. B* **81**, 165441 (2010).
- [9] V. A. Shalygin, M. D. Moldavskaya, S. N. Danilov, I. I. Farbshtein, and L. E. Golub, *Phys. Rev. B* **93**, 045207 (2016).
- [10] J. E. Goff and W. L. Schaich, *Phys. Rev. B* **56**, 15421 (1997); **61**, 10471 (2000).
- [11] M. Durach, A. Rusina, and M. I. Stockman, *Phys. Rev. Lett.* **103**, 186801 (2009).
- [12] T. Hatano, T. Ishihara, S. G. Tikhodeev, and N. A. Gippius, *Phys. Rev. Lett.* **103**, 103906 (2009).
- [13] M. Durach and N. Noginova, *Phys. Rev. B* **93**, 161406 (2016).

- [14] W. Gao, M. Lawrence, B. Yang, F. Liu, F. Fang, B. Béri, J. Li, and S. Zhang, *Phys. Rev. Lett.* **114**, 037402 (2015).
- [15] M. Onoda and T. Ochiai, *Phys. Rev. Lett.* **103**, 033903 (2009).
- [16] K. Sawada, S. Murakami, and N. Nagaosa, *Phys. Rev. Lett.* **96**, 154802 (2006).
- [17] Y. Kohmura, K. Sawada, and T. Ishikawa, *Phys. Rev. Lett.* **104**, 244801 (2010).
- [18] Y. Kohmura, K. Sawada, S. Fukatsu, and T. Ishikawa, *Phys. Rev. Lett.* **110**, 057402 (2013).
- [19] See Supplemental Material at <http://link.aps.org/supplemental/10.1103/PhysRevLett.117.083901> for the derivation of the nonlinear current.
- [20] H. Kurosawa and T. Ishihara, *Opt. Express* **20**, 1561 (2012).
- [21] H. Kurosawa, T. Ishihara, N. Ikeda, M. Ochiai, and Y. Sugimoto, *Opt. Lett.* **37**, 2793 (2012).
- [22] T. Hatano, B. Nishikawa, M. Iwanaga, and T. Ishihara, *Opt. Express* **16**, 8236 (2008).
- [23] S. G. Tikhodeev, A. L. Yablonskii, E. A. Muljarov, N. A. Gippius, and T. Ishihara, *Phys. Rev. B* **66**, 045102 (2002).
- [24] L. Li, *J. Opt. Soc. Am. A* **13**, 1024 (1996); **14**, 2758 (1997).